THE JOURNAL OF CHEMICAL PHYSICS **129**, 034107 (2008)

Simultaneous benchmarking of ground- and excited-state properties with long-range-corrected density functional theory

Mary A. Rohrdanz and John M. Herbert[a)]
Department of Chemistry, The Ohio State University, Columbus, Ohio 43210, USA

(Received 19 May 2008; accepted 12 June 2008; published online 21 July 2008)

We present benchmark calculations using several long-range-corrected (LRC) density functionals, in which Hartree–Fock exchange is incorporated asymptotically using a range-separated Coulomb operator, while local exchange is attenuated using an *ansatz* introduced by Iikura *et al.* [J. Chem. Phys. **115**, 3540 (2001)]. We calculate ground-state atomization energies, reaction barriers, ionization energies, and electron affinities, each as a function of the range-separation parameter μ. In addition, we calculate excitation energies of small- and medium-sized molecules, again as a function of μ, by applying the LRC to time-dependent density functional theory. Representative examples of both pure and hybrid density functionals are tested. On the basis of these results, there does not appear to be a single range-separation parameter that is reasonable for both ground-state properties and vertical excitation energies. Reasonable errors in atomization energies and barrier heights are achieved only at the expense of excessively high excitation energies, at least for the medium-sized molecules, whereas values of μ that afford reasonable excitation energies yield some of the largest errors for ground-state atomization energies and barrier heights in small molecules. Notably, this conclusion is obscured if the database of excitation energies includes only small molecules, as has been the case in previous benchmark studies of LRC functionals. © *2008 American Institute of Physics*. [DOI: 10.1063/1.2954017]

I. INTRODUCTION

Over the past few years, several groups have explored a type of long-range-corrected (LRC) density functional theory (DFT) in which Hartree–Fock (HF) exchange is turned on—and DFT exchange is turned off—asymptotically.[1–17] Such methods attempt to correct the long-range behavior of the exchange-correlation potential $v_{xc}(\mathbf{r})$ and are motivated by the observation that only full HF exchange properly describes the distance dependence of long-range charge-transfer (CT) excitation energies.[18] As such, elimination of spurious CT states in time-dependent DFT (TD-DFT) often requires a coefficient of HF exchange that is significantly larger than the coefficients employed in popular hybrid functionals.[19,20]

At some level, each of these LRC schemes relies on a partition of the Coulomb operator into short- and long-range components. The simplest form of this partition is

$$\frac{1}{r} = \frac{1-\mathrm{erf}(\mu r)}{r} + \frac{\mathrm{erf}(\mu r)}{r}, \tag{1}$$

in which "erf" denotes the error function. The first term on the right of Eq. (1) is a short-range Coulomb operator that decays to zero on a length scale of $\sim 1/\mu$, where μ is considered to be an adjustable parameter. The second term dominates the first at large r, and thus corresponds to a "long-range" or "background" part of the Coulomb operator. (Note that both components increase monotonically as $r \to 0$, but the short-range component dominates the background term at small r.)

In LRC-DFT, the partitioned or "range-separated" Coulomb operator in Eq. (1) is used to evaluate the exchange energy. Consider an exchange-correlation functional of the form

$$E_{xc} = E_c + (1 - C_{HF})E_{x,\mathrm{local}} + C_{HF}E_{x,HF}, \tag{2}$$

in which C_{HF} represents the coefficient of HF exchange, $0 \leqslant C_{HF} \leqslant 1$. Then the LRC exchange-correlation energy for this functional takes the form

$$E_{xc}^{LRC} = E_c + (1 - C_{HF})E_{x,\mathrm{local}}^{SR} + C_{HF}E_{x,HF}^{SR} + E_{x,HF}^{LR}, \tag{3}$$

where $E_{x,HF}^{SR}$ and $E_{x,HF}^{LR}$ denote the HF exchange energy evaluated using the short- and long-range components of the Coulomb operator, respectively, and $E_{x,\mathrm{local}}^{SR}$ denotes the local DFT exchange energy evaluated using the short-range part of the Coulomb operator. The correlation energy E_c is not modified. The LRC functional in Eq. (3) recovers standard DFT [Eq. (2)] in the limit that $\mu \to 0$, whereas the $\mu \to \infty$ limit corresponds to a new functional, $E_{xc} = E_c + E_{x,HF}$.

Evaluation of $E_{x,HF}^{SR}$ and $E_{x,HF}^{LR}$ is straightforward using modified exchange integrals,[21] but the form of $E_{x,\mathrm{local}}^{SR}$ depends on the form of the local exchange functional, and two different *ansätze* have been proposed from which to construct a short-range version of $E_{x,\mathrm{local}}$. One scheme (introduced by Hirao and co-workers[2–5]) is based on a modified exchange energy density, while the other strategy (developed by Scuseria and co-workers[9–12]) employs a modified exchange hole. In this work, we focus exclusively on the Hirao model, which to date has seen more widespread application.

[a)] Electronic mail: herbert@chemistry.ohio-state.edu.

A major aim of LRC-DFT is to correct long-range CT problems in TD-DFT without contaminating the short-range part of $v_{\mathrm{xc}}(\mathbf{r})$ with extra HF exchange, which might seriously degrade DFT's performance for properties that do not depend on the tail of this potential. The LRC (in either of the *ansätze* described above) provides the correct asymptotic distance dependence for CT excitations in TD-DFT,[2,3,10,17] and at the same time rectifies certain problems with ground-state DFT, such as bond-dissociation potentials for cation dimers that diverge at large separation.[9,17] We have recently shown[16] that LRC functionals remove the near continuum of spurious, low-energy CT excitations that contaminate TD-DFT calculations in clusters and condensed phases.[22]

Given any pure or hybrid density functional, LRC-DFT introduces one additional parameter μ that is usually adjusted in order to minimize statistical errors in atomization energies, barrier heights, ionization energies, and other ground-state properties.[2,3,9,10,17] As expected, however, CT excitation energies are exquisitely sensitive to the value of μ (tunable over a range of more than 2 eV, as a function of μ, in one recent application[16]), and it is unclear *a priori* whether the statistically optimal value of μ for ground-state properties is also reasonable for excitation energies computed using TD-DFT.

In the present work, we address this issue via simultaneous benchmarking of both ground-state properties (atomization energies, barrier heights, ionization energies, and electron affinities) and vertical excitation energies. We analyze the μ-dependence of each of these properties, for both small- and medium-sized molecules. Our approach differs from that employed in previous benchmark studies of LRC-DFT, in which μ is optimized in order to minimize statistical errors in various ground-state properties,[2,3,9,10,17] or occasionally, ground-state properties plus small-molecule vertical excitation energies.[5,15] While there have been some preliminary indications that ground- and excited-state properties might exhibit different optimal values for μ,[5,15] the μ-dependence of vertical excitation energies has not yet been examined in a systematic way for molecules much larger than H_2CO or CH_3CO. Instead, applications of TD-LRC-DFT to large molecules have so far relied on the values of μ that are optimized for ground-state properties.[23–25]

Here, we present the first systematic investigation of the μ-dependence of vertical excitation energies in larger molecules, while simultaneously examining the μ-dependence of ground-state properties. Our results suggest that there is no value of μ that is simultaneously optimal (or nearly optimal) both for ground-state properties such as atomization energies and reaction barrier heights, as well as for vertical excitation energies in moderately large organic chromophores.

II. THEORY AND METHODOLOGY

We have implemented the LRC procedure as described by Hirao and co-workers,[2,3] for both pure and hybrid density functionals, within a developers' version of Q-CHEM.[26] Calculation of the HF exchange energies $E_{\mathrm{x,HF}}^{\mathrm{SR}}$ and $E_{\mathrm{x,HF}}^{\mathrm{LR}}$ in Eq. (3) requires exchange integrals with respect to the modified Coulomb operators, and these integrals have been implemented in Q-CHEM by Adamson *et al.*[21]

The quantity $E_{\mathrm{x,local}}^{\mathrm{SR}}$ is evaluated by quadrature. For the version of LRC-DFT proposed by Hirao and co-workers,[2,3] the short-range exchange energy is given by

$$E_{\mathrm{x,local}}^{\mathrm{SR}} = -\frac{1}{2}\sum_{\sigma}\int d\mathbf{r}\,\rho_{\sigma}^{4/3}(\mathbf{r})K_{\sigma}^{\mathrm{GGA,SR}}(\mathbf{r}), \tag{4}$$

in which $K_{\sigma}^{\mathrm{GGA,SR}}$ is the short-range analog of $K_{\sigma}^{\mathrm{GGA}}$, the exchange kernel for σ spin. The quantity $K_{\sigma}^{\mathrm{GGA}}$ is defined by the choice of generalized gradient approximation (GGA), and Hirao and co-workers[2,3] provide a prescription for deriving the $K_{\sigma}^{\mathrm{GGA,SR}}$ corresponding to any given $K_{\sigma}^{\mathrm{GGA}}$. (The implementation of $K_{\sigma}^{\mathrm{GGA,SR}}$ described in Ref. 3 is numerically more stable than the one in Ref. 2, so we employ the former.)

The dependence of Eq. (4) on the short-range part of the Coulomb operator is not obvious but is folded into the prescription for obtaining $K_{\sigma}^{\mathrm{GGA,SR}}$. As shown in Ref. 2 (see also Ref. 1), the "exchange-kernel" formulation of $E_{\mathrm{x,local}}^{\mathrm{SR}}$ in Eq. (4) is formally equivalent to

$$E_{\mathrm{x,local}}^{\mathrm{SR}} = -\frac{1}{2}\sum_{\sigma}\int d\mathbf{R}d\mathbf{r}\left(\frac{1-\mathrm{erf}(\mu r)}{r}\right) \times |P_{\sigma}^{\mathrm{GGA}}(\mathbf{R}+\mathbf{r}/2,\mathbf{R}-\mathbf{r}/2)|^2, \tag{5}$$

in which $P_{\sigma}^{\mathrm{GGA}}$ represents the one-electron exchange density matrix for σ spin, for the particular GGA in question. The density-matrix formulation of $E_{\mathrm{x,local}}^{\mathrm{SR}}$ in Eq. (5) makes explicit the appearance of the short-range Coulomb operator, $[1-\mathrm{erf}(\mu r)]/r$.

We have so far implemented short-range versions of Becke88 exchange[27] and Perdew–Burke–Ernzerhof (PBE) exchange,[28] from which LRC variants of many common density functionals may be constructed. These include PBE,[28] PBE0,[29] BLYP,[27,30] BOP,[31] and PBEOP.[31] These functionals and their LRC variants are available in the developers' version of Q-CHEM. Here, we focus on LRC versions of the popular functionals PBE, BLYP, and PBE0, as representative examples of both pure and hybrid density functionals.

Ground-state calculations reported here use the aug-cc-pVTZ basis set, with geometries obtained from the Minnesota Thermochemistry and Thermochemical Kinetics Database.[32,33] Excitation energies are calculated using the aug-cc-pVDZ basis set. We find that excitation energies of low-lying transitions computed at the TD-DFT/aug-cc-pVDZ level generally differ by no more than 0.02 eV from the results obtained with the aug-cc-pVTZ basis set, so the smaller basis is used here for excitation energies. (Results comparing several basis sets are available in the Supporting Information.[34]) All calculations use the SG-1 quadrature grid.[35] For the small-molecule excitation energy benchmarks, geometries were taken from the NIST database,[36] while geometries for the larger molecules were optimized at the B3LYP/6-31G* level. The Tamm–Dancoff approximation was not used for any of these calculations. All properties were calculated for μ ranging from zero to $0.90a_0^{-1}$, in incre-

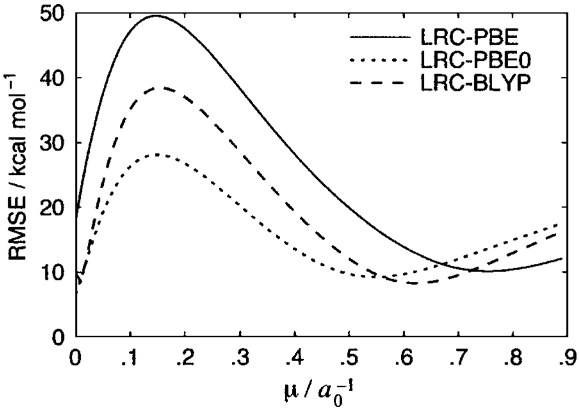

FIG. 1. RMSEs for atomization energies as a function of the range parameter μ. For comparison, the B3LYP ($\mu=0$) RMSE is 7.0 kcal/mol with the same basis set and grid.

ments of $0.01a_0^{-1}$, where a_0 denotes the Bohr radius. (Values larger than $0.90a_0^{-1}$ yield large errors in some ground-state and most excited-state properties.)

III. RESULTS

A. Ground-state benchmarks

Benchmark thermochemical values were obtained from the Minnesota Thermochemistry and Thermochemical Kinetics Database (specifically, Database 3),[32,33] and include atomization energies for 109 molecules,[37] forward and reverse barrier heights for 22 reactions,[38] and the ionization energies and electron affinities of 13 species.

Figure 1 displays root-mean-square errors (RMSEs) for atomization energies as a function of the range-separation parameter μ. For each of the LRC functionals, adding a small amount of long-range HF exchange $(0<\mu\lesssim 0.2a_0^{-1})$ yields significant errors in comparison with the "base" functional, i.e., the functional with $\mu=0$. For the pure functionals, larger values of μ prove optimal: for LRC-PBE, $\mu=0.75a_0^{-1}$ outperforms the base functional, as does LRC-BLYP with $\mu=0.62a_0^{-1}$. In contrast, LRC-PBE0 does not exhibit any value of μ that outperforms the base functional.

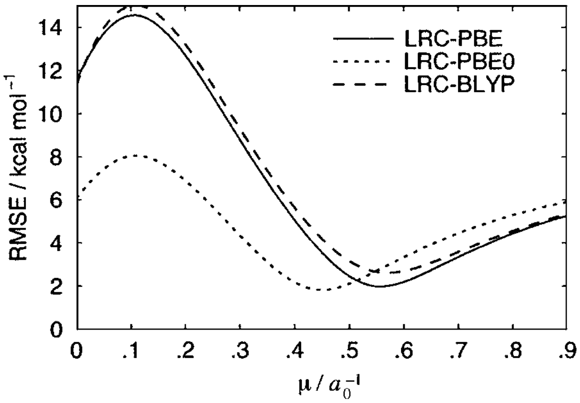

FIG. 2. RMSEs for forward and reverse barrier heights as a function of the range parameter μ. For the optimal μ values, the LRC functional outperforms both the corresponding base functional and B3LYP ($\mu=0$), which affords a RMSE of 7.7 kcal/mol for the same basis set and grid.

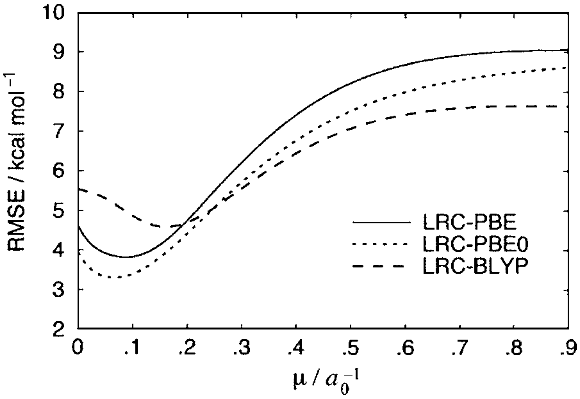

FIG. 3. RMSEs for ionization energies as a function of the range parameter μ. The optimal μ values are considerably smaller than those for atomization energies and barrier heights. The RMSE for B3LYP ($\mu=0$) is 5.7 kcal/mol with the same basis set and grid.

The data for barrier heights are displayed in Fig. 2. The trend among RMSEs is qualitatively similar to that observed for atomization energies. In particular, the pure functionals exhibit larger RMSEs at small μ than does the hybrid, which is consistent with their behavior at $\mu=0$. One difference relative to the atomization energies is that LRC-PBE0 does exhibit a value of $\mu>0$ that statistically outperforms PBE0.

The RMSEs for ionization energies and electron affinities exhibit markedly different μ-dependence than the atomization energies and barrier heights. For ionization energies (Fig. 3), $\mu\sim 0.1-0.2a_0^{-1}$ performs slightly better than the base functional. Regarding electron affinities (Fig. 4), LRC versions of the two pure functionals once again show similar behavior to one another, and outperform their $\mu=0$ counterparts in the range $\mu=0.53-0.56a_0^{-1}$. For LRC-PBE0, the lowest RMSE is obtained at $\mu=0.32a_0^{-1}$.

B. Small-molecule excitation energies

Next, we consider vertical electronic excitation energies for three standard benchmark molecules: CO, H_2CO, and CH_3CHO. These excitation energies are depicted (as functions of μ) in Figs. 5–7, respectively. In each figure, the results from LRC-PBE are shown in panel (a) and the results from LRC-PBE0 are shown in panel (b). For carbon monoxide, the experimental values (indicated by the horizontal

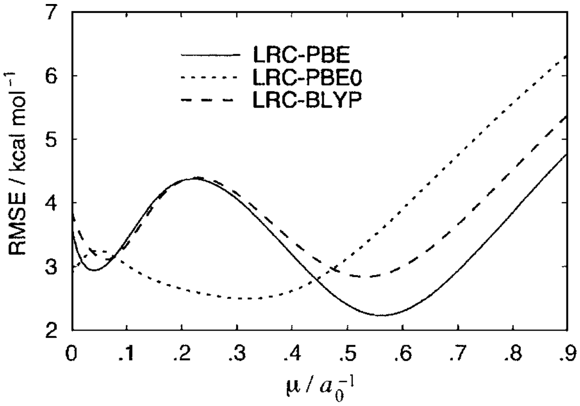

FIG. 4. RMSEs for electron affinities as a function of the range parameter μ. The RMSE for B3LYP ($\mu=0$) is 3.7 kcal/mol with the same basis set and grid.

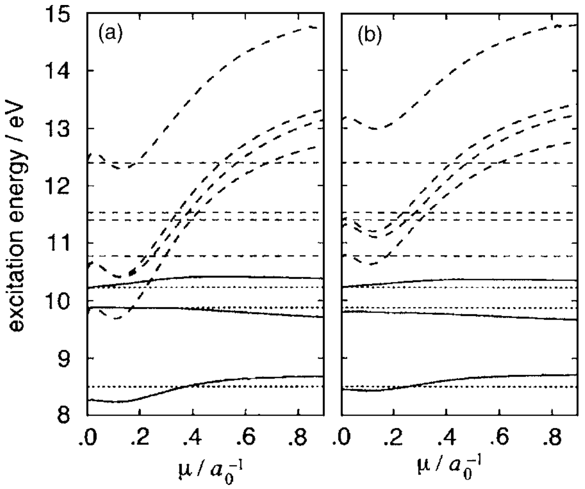

FIG. 5. TD-DFT vertical excitation energies for carbon monoxide for (a) LRC-PBE and (b) LRC-PBE0. The Rydberg excitation energies (dashed curves) exhibit a stronger μ dependence than the valence excitation energies (solid curves). The horizontal dotted lines are experimental valence excitation energies, and horizontal dashed lines are experimental Rydberg excitation energies (Ref. 41).

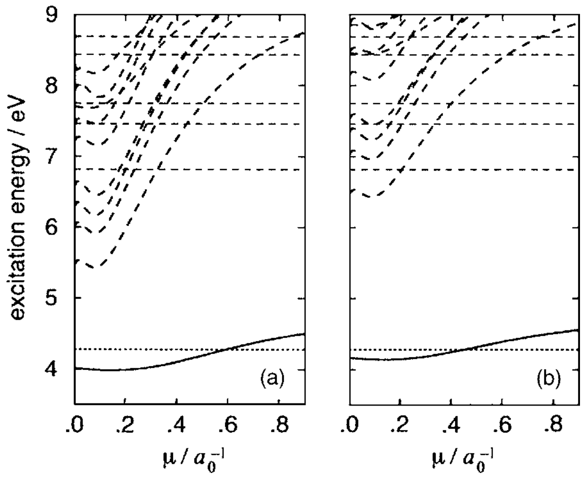

FIG. 7. TD-DFT vertical excitation energies for acetaldehyde for (a) LRC-PBE and (b) LRC-PBE0. The Rydberg excitation energies (dashed curves) exhibit a stronger μ dependence than the valence excitation energies (solid curves). The horizontal dotted lines are experimental valence excitation energies, and horizontal dashed lines are experimental Rydberg excitation energies (Ref. 40).

lines) have had zero-point energy removed, so that direct comparison with our calculated values is appropriate. For H_2CO and CH_3CO, the experimental excitation energies represent peak maxima in electron impact spectra,[39] and (consistent with previous theoretical studies[40]) we will compare these values directly to TD-DFT vertical excitation energies. As observed with CT excitations in our previous work,[16] we observe that Rydberg excitation energies (depicted as dashed curves in the figures) are strongly μ-dependent, whereas valence excitations (solid curves) are not.

As an example, consider the LRC-PBE results for CO [Fig. 5(a)]. For this molecule, the lowest-energy valence excitation ranges from 8.24 eV (μ=0.11a_0^{-1}) to 8.69 eV (μ=0.90a_0^{-1}) for an overall variation of 0.44 eV. This is within the 0.3–0.5 eV error bar that is usually ascribed to TD-DFT valence excitation energy predictions.[42] The next two valence transitions span energy ranges of 0.18 and 0.21 eV, well within the intrinsic accuracy of contemporary TD-DFT. On the other hand, the lowest-energy Rydberg excitation energy ranges from 9.69 eV (μ=0.11a_0^{-1}) to 12.70 eV (μ=0.90a_0^{-1}), a variation of ~3 eV.

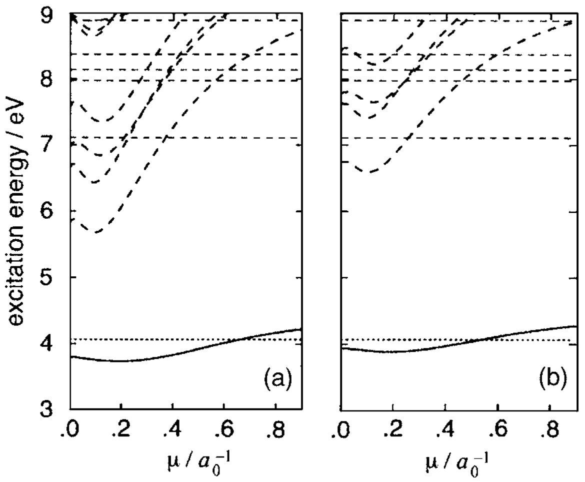

FIG. 6. TD-DFT vertical excitation energies for formaldehyde for (a) LRC-PBE and (b) LRC-PBE0. The Rydberg excitation energies (dashed curves) exhibit a stronger μ dependence than the valence excitation energies (solid curves). The horizontal dotted lines are experimental valence excitation energies, and horizontal dashed lines are experimental Rydberg excitation energies (Ref. 40).

CO excitation energies calculated using LRC-PBE0 are shown Fig. 5(b). Here, the overall variation in the excitation energies is slightly smaller than for LRC-PBE (≈0.2–0.3 eV for the valence excitations and ~2 eV for the Rydberg transitions), but the trend is the same: weak μ-dependence for the valence transitions, with larger μ-dependence for Rydberg transitions.

Formaldehyde and acetaldehyde show similar trends. Additionally, LRC variants of the functionals BLYP,[27,30] BOP,[31] and PBEOP (Ref. 31) afford results that are qualitatively similar to those obtained using LRC-PBE. Graphs of the μ-dependent excitation energies of carbon monoxide predicted by these functionals are available in the Supporting Information.[34]

C. Larger-molecule excitation energies

We have also examined selected excitations in the larger organic chromophores depicted in Fig. 8, namely, $\pi \rightarrow \pi^*$ transitions in anthracene and indole, $n \rightarrow \pi^*$ excitations in pyridazine, benzocyclobutenedione, and benzaldehyde, and Rydberg transitions in pyrrole. For these particular molecules and excitations, reliable vertical excitation energy estimates are available from experiment.[43] Consistent with Ref. 43, we compare TD-DFT vertical excitation energies directly against experimental band maxima. (Any small error arising from this approximation is likely insignificant in comparison to the strong μ-dependence that we observe in the predicted excitation energies.)

Figures 9–14 display the results of calculations with LRC-PBE (left panel), and LRC-PBE0 (right panel) for these molecules. The symmetry labels attached to each transition

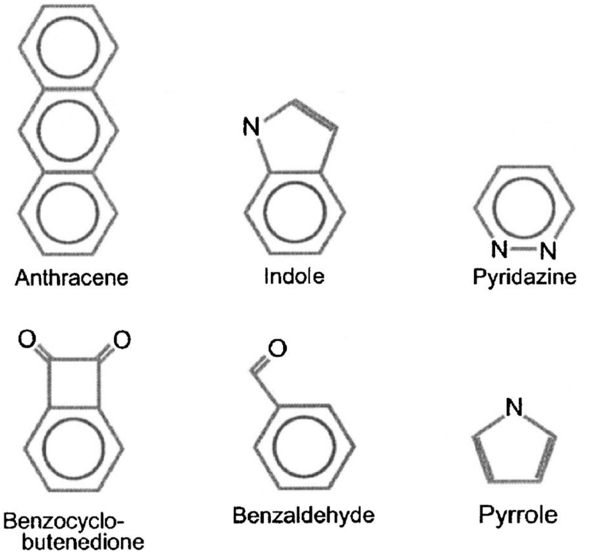

FIG. 8. Structures of the organic chromophores whose excited states are examined in this work.

correspond to the molecular orientation given in Ref. 44. The horizontal lines in each figure are experimental estimates of the excitation energies,[43] while the curved lines show the results of our calculations as functions of μ. The experimental estimates are zero-point adjusted such that comparison with our calculations is appropriate.[43] It should be noted that for many of these molecules, transitions other than those displayed in the figures do exist within the energy window shown in the figure, but for clarity we show only those excitations for which experimental data were reported in Ref. 43. For most of the molecules, the graph for LRC-BLYP is nearly identical to that shown for LRC-PBE, with the only exception being the Rydberg transitions of pyrrole. The LRC-BLYP excitations for each molecule are available in the Supporting Information.[34]

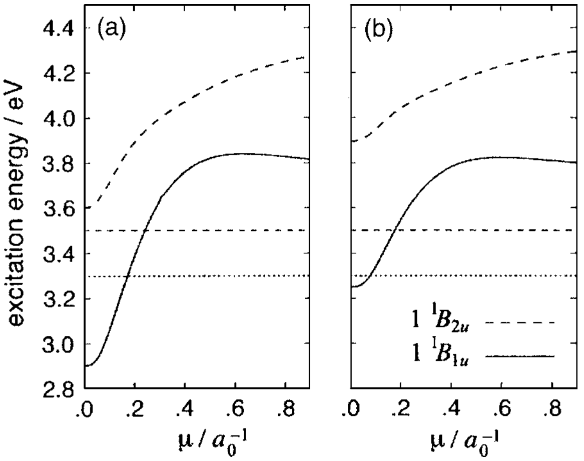

FIG. 9. The two lowest excitations (both $\pi\rightarrow\pi^*$) for anthracene using (a) LRC-PBE and (b) LRC-PBE0. The solid curve represents the $1\ ^1B_{1u}$ state and the dashed curve is the $1\ ^1B_{2u}$ state. The horizontal lines are from experiment (Ref. 43) with the dotted line representing the $1\ ^1B_{1u}$ excitation energy and the dashed line representing $1\ ^1B_{2u}$.

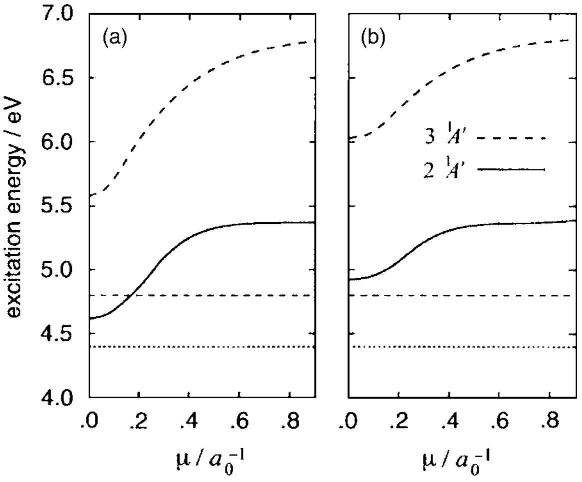

FIG. 10. Two $\pi\rightarrow\pi^*$ excitations for indole calculated using (a) LRC-PBE and (b) LRC-PBE0. The horizontal lines represent experimental values (Ref. 43).

In contrast to the small-molecule results in the previous section, for these larger chromophores, even the valence excitations exhibit a strong dependence on the range parameter. The $\pi\rightarrow\pi^*$ transitions generally exhibit a rapid increase in excitation energy as μ increases from zero to $\sim 0.4a_0^{-1}$, followed by a leveling off. In the case of anthracene $\pi\pi^*$ states (Fig. 9),[45] the LRC-PBE vertical excitation energies span a range of 0.9 eV for the $1\ ^1B_{1u}$ state ("L_a") and 0.7 eV for the $1\ ^1B_{2u}$ state ("L_b"). Both values are larger than anticipated TD-DFT errors for low-lying valence excitations.[42] The LRC-PBE0 results span slightly smaller ranges, 0.6 eV for $1\ ^1B_{1u}$, and 0.4 eV for $1\ ^1B_{2u}$. By the time μ reaches $0.9a_0^{-1}$, the LRC-PBE and LRC-PBE0 excitation energies are quite comparable, indicating that this is close to the $\mu\rightarrow\infty$ limit, in which $E_{\mathrm{xc}}\rightarrow E_{\mathrm{c}}+E_{\mathrm{x,HF}}$.

The $\pi\pi^*$ states in indole (Fig. 10) afford a similar picture. Over the range $0\leqslant\mu\leqslant 0.9a_0^{-1}$, the excitation energy for the $2\ ^1A'$ state (L_b) spans a range of 0.8 eV when using LRC-PBE, or 0.5 eV for LRC-PBE0. For the $3\ ^1A'$ state (L_a), the variation is even larger: 1.2 eV for LRC-PBE and 0.8 eV for LRC-PBE0. Both functionals once again afford similar excitation energies for $\mu=0.90a_0^{-1}$. No value of μ improves upon the excitation energies predicted using $\mu=0$.

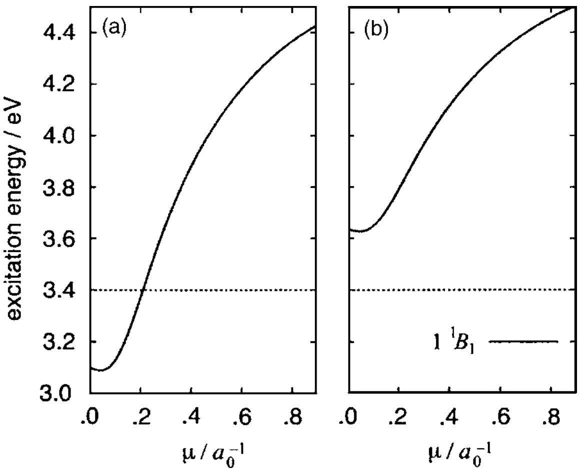

FIG. 11. The lowest excitation energy for pyridazine, representing the $1\ ^1B_1$ ($n\pi^*$) state, for (a) LRC-PBE and (b) LRC-PBE0. The horizontal line represents the experimental value (Ref. 43).

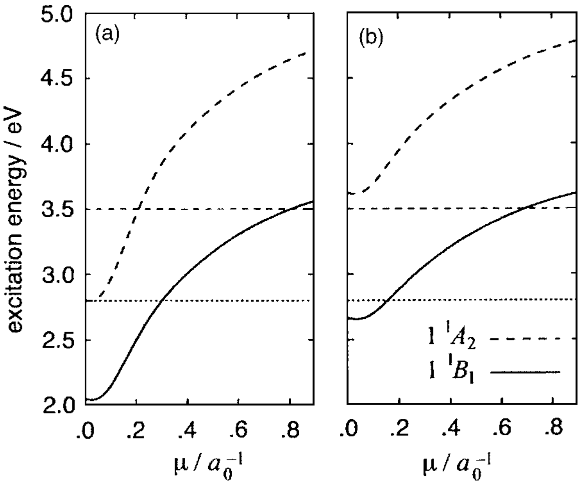

FIG. 12. The two lowest excitation energies (both $n\rightarrow\pi^*$) for benzocyclobutenedione using (a) LRC-PBE and (b) LRC-PBE0. The horizontal lines indicate the experimental values (Ref. 43) with the dotted line representing the $1\ {}^1B_1$ excitation energy and the dashed line representing $1\ {}^1A_2$.

The $n\rightarrow\pi^*$ excitation energies for pyridazine (Fig. 11), benzocyclobutenedione (Fig. 12), and benzaldehyde (Fig. 13) show a slightly different trend. Rather than plateauing at larger values of μ, these excitation energies exhibit a more steady increase as μ increases. (Previously, we observed the same contrasting behavior between $n\pi^*$ and $\pi\pi^*$ states in a single system, namely, a π-stacked adenine dimer.[16]) For each of these three molecules, the $n\rightarrow\pi^*$ excitation energies calculated with LRC-PBE0 span a range of about 1 eV, while LRC-PBE excitation energies span an even larger range. In all cases, this variation is much larger than the error bar typically ascribed to TD-DFT predictions of the lowest few valence excitations.[42]

Two low-lying Rydberg excitations of pyrrole are shown in Fig. 14. These excitation energies each vary over 1.8 eV in the case of LRC-PBE and 1.3 eV in the case of LRC-PBE0. These variations are somewhat larger than than those observed for valence excitation energies of the other molecules discussed in this section; however, the difference between the μ-dependence of valence and Rydberg excitation energies is no longer so pronounced as it was for the small molecules discussed in Sec. III B.

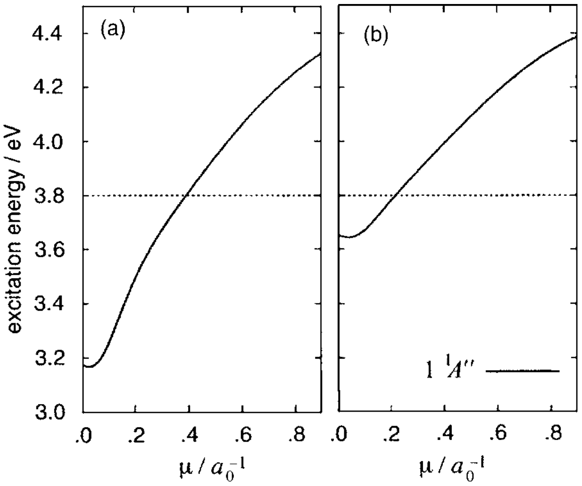

FIG. 13. The lowest excitation energy for benzaldehyde (an $n\pi^*$ state, $1\ {}^1A''$) using (a) LRC-PBE and (b) LRC-PBE0. The horizontal line represents the experimental value (Ref. 43).

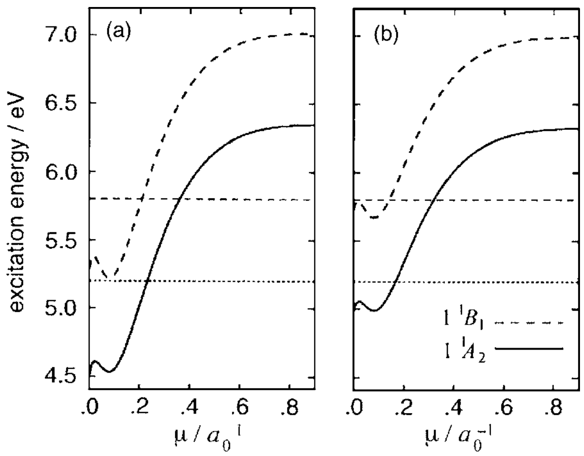

FIG. 14. The two lowest Rydberg excitations for pyrrole, $1\ {}^1A_2$ and $1\ {}^1B_1$, using (a) LRC-PBE and (b) LRC-PBE0. The horizontal lines represent the experimental values (Ref. 43) with the dotted line representing the $1\ {}^1A_2$ excitation energy and the dashed line representing $1\ {}^1B_1$.

IV. DISCUSSION

Several previous studies have reported on LRC functionals in which the range-separation parameter μ in Eq. (1), which is sometimes denoted as ω instead of μ, is optimized in order to minimize statistical errors in various ground-state properties. Song *et al.*,[3] for example, suggest a value of $0.47a_0^{-1}$ for the LRC-BOP functional. Chai and Head-Gordon[17] have reoptimized *all* parameters (including those of the base functional) in a LRC version of the B97 functional[46] that they term ωB97, and also in an analogous hybrid functional that they denote as ωB97X. These authors report optimal values of $\mu=0.4a_0^{-1}$ for ωB97 and $\mu=0.3a_0^{-1}$ for ωB97X. Of these functionals, LRC-BOP and ωB97 are based on pure functionals ($C_{\mathrm{HF}}=0$), as are LRC-PBE and LRC-BLYP in the present work, whereas ωB97X and LRC-PBE0 are based on hybrids ($C_{\mathrm{HF}}>0$). Note that the hybrid functional ωB97X exhibits a smaller optimal value of μ that does ωB97, owing to the presence of short-range HF exchange in the former.

Our ground-state benchmarks afford optimal μ values that are basically in line with (though somewhat larger than) the values suggested in the aforementioned studies, with the differences attributable to the use of different base functionals and slightly different training sets. Our excited-state calculations, on the other hand, suggest a much smaller value of μ is appropriate for TD-DFT. Tables I and II list the optimal

TABLE I. Optimal values of μ (in a_0^{-1}) for ground-state properties.

	LRC-BLYP	LRC-PBE	LRC-PBE0
Atomization energy	0.62	0.75	0.55
Barrier heights	0.57	0.56	0.45
Ionization energies	0.16	0.09	0.07
Electron affinities	0.53	0.56	0.32

TABLE II. Optimal values of μ (in a_0^{-1}) for excitation energies.

	LRC-BLYP	LRC-PBE	LRC-PBE0
Anthracene			
$1\,^1B_{1u}$ ($\pi\pi^*$)	0.18	0.18	0.08
$1\,^1B_{2u}$ ($\pi\pi^*$)	0.00	0.00	0.00
Indole			
$2\,^1A'$ ($\pi\pi^*$)	0.00	0.00	0.00
$3\,^1A'$ ($\pi\pi^*$)	0.00	0.00	0.00
Pyridazine			
$1\,^1B_1$ ($n\pi^*$)	0.20	0.21	0.05
Benzocyclo-butendione			
$1\,^1B_1$ ($n\pi^*$)	0.29	0.30	0.16
$1\,^1A_2$ ($n\pi^*$)	0.20	0.21	0.03
Benzaldehyde			
$1\,^1A''$ ($n\pi^*$)	0.37	0.39	0.22
Pyrrole			
$1\,^1A_2$ (Rydberg)	0.30	0.23	0.17
$1\,^1B_1$ (Rydberg)	0.27	0.21	0.14

μ values for ground- and excited-state properties, respectively, as determined from the data in Sec. III.

The most salient features of our results are (i) the difference between the optimal values of μ for ground- versus excited-state properties, (ii) the difference in μ-dependence for valence versus Rydberg excitations in small molecules, and (iii) the difference in μ-dependence for small- versus large-molecule valence excitation energies. Each of these differences is addressed below. For brevity we restrict our discussion to LRC-PBE and LRC-PBE0, but data for LRC-BLYP can be found in the Supporting Information.[34]

In comparing Tables I and II, stark differences are seen between the optimal range parameter for atomization energies, barrier heights, and electron affinities, on the one hand, and for ionization energies and excitation energies on the other. The general trend is that the optimal value of μ for the latter properties is considerably smaller than the optimal value for the former. Large errors in excitation energies are obtained at the value of μ that is optimal for atomization energies and barrier heights, and vice versa. In the case of LRC-PBE, for example, a value $\mu \lesssim 0.4a_0^{-1}$ is necessary to avoid large errors in excitation energies, but unless μ is very close to zero [corresponding to very little LRC, and thus severe problems with CT contamination in TD-DFT (Ref. 16)], such a small value of μ engenders errors of more than 30 kcal/mol in atomization energies. On the other hand, for $\mu \approx 0.6a_0^{-1}$ (optimal for most ground-state properties), there are significant errors for excitation energies. For LRC-PBE, $\mu = 0.6a_0^{-1}$ yields errors larger than 0.5 eV (and typically closer to 1 eV) for all but one of the large-molecule excitations considered here. Similar trends are observed for LRC-PBE0, although the optimal values of μ tend to be slightly smaller than for LRC-PBE, consistent with the presence of short-range exchange in LRC-PBE0.

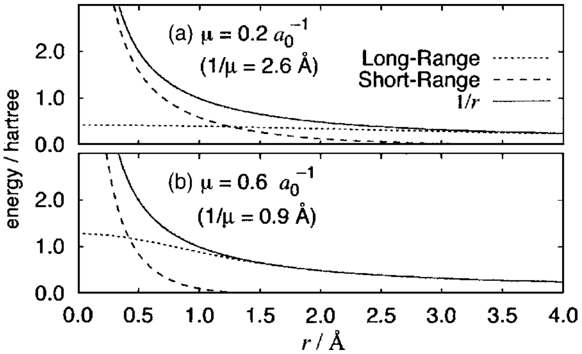

FIG. 15. Comparison of the short- and long-range components of the Coulomb potential for two values of the range-separation parameter, μ.

The difference in μ-dependence between ground- and excited-state properties may arise in part due to the size of the molecules in each of the various data sets. For the atomization energy calculations, our data set consists mostly of small polyatomic molecules a few angstroms in size, whereas the aromatic chromophores surveyed by TD-DFT in Sec. III C are each 4–9 Å in length. It is perhaps enlightening, then, to consider molecular size in comparison to the length scale, $1/\mu$, on which DFT exchange is attenuated. Figure 15 plots the long- and short-range components of $1/r$ for two different values of μ. For a molecule that is 2 Å in length and using a value of $\mu = 0.2a_0^{-1}$ ($1/\mu = 2.6$ Å), the short-range Coulomb operator does not fully decay to zero on the length scale of the molecule, whereas for $\mu = 0.6a_0^{-1}$ ($1/\mu = 0.9$ Å), the short-range part of $1/r$ dies off on a length scale shorter than the molecule. On the other hand, if the molecule is 4 Å in extent, the short-range part of $1/r$ decays to zero on a length scale shorter than the length of the molecule, even for $\mu = 0.2a_0^{-1}$. This may be important with respect to error cancellation: if there is a delicate balance between exchange and correlation errors, we might expect the amount of DFT exchange within the length of the molecule to affect the final errors.

The second key point is the different behavior of valence versus Rydberg excitations for small molecules, which is almost certainly an issue of length scales. The effective size of a molecule changes very little upon valence excitation but can increase considerably upon Rydberg excitation. Consequently, an electron excited to a Rydberg orbital experiences a very different part of $v_{\mathrm{xc}}(\mathbf{r})$ than does an electron excited from an occupied valence orbital into a valence π^* orbital. We further note that, among the ground-state properties considered here, the trend in RMSEs versus μ for ionization energies (Fig. 3) most closely resembles the trend for small-molecule Rydberg excitation energies (Figs. 5–7). This result is consistent with the idea that ionization corresponds to a Rydberg excitation into an orbital with principal quantum number $n = \infty$.

The third key point is the disappearance of the dichotomy between valence and Rydberg excitations in larger molecules. In small molecules, Rydberg excitation energies are strongly μ-dependent but valence excitation energies are only weakly μ-dependent, whereas for larger molecules all of the excitation energies are quite sensitive to μ. For example, in the CO molecule the lowest valence excitation energy shifts by 0.44 eV between $\mu = 0$ and $\mu = 0.9a_0^{-1}$, and while this shift is not exactly small, it is (just) within the

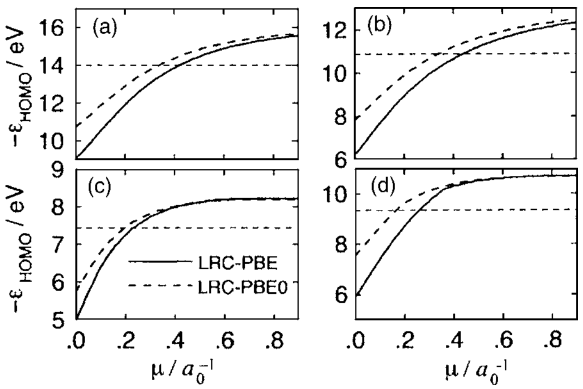

FIG. 16. Plots of $-\varepsilon_{\mathrm{HOMO}}$ for (a) carbon monoxide, (b) formaldehyde, (c) anthracene, and (d) benzaldehyde. Horizontal lines indicate the experimental ionization energies (Ref. 49).

accepted intrinsic error bar for valence excitation energy predictions in TD-DFT.[42] In comparison, the lowest excitation energies in anthracene and benzocyclobutenedione shift by 0.90 and 1.52 eV, respectively, over the same range of μ. For small molecules, there is a clear separation of length scales between valence and Rydberg excitations, and the valence excited-state densities essentially fit underneath the $[1\text{-erf}(\mu r)]/r$ envelope of short-range DFT exchange. As molecular size increases, however, this clear separation of length scales breaks down, as even valence excitations may involve orbitals that sample both the long- and short-range parts of the Coulomb operator.

Although TD-DFT excitation energies are typically reasonably accurate for the lowest few valence excited states, those for higher-lying excited states are typically underestimated by standard functionals.[42,47] The negative of the highest occupied molecular orbital (HOMO) energy, $-\varepsilon_{\mathrm{HOMO}}$, is considered to be the cutoff between "low-lying" and "higher-lying."[48] The errors in high-energy excited states have been ascribed to the incorrect asymptotic behavior of the exchange correlation potential, and linked to an underestimation of the ionization energy, which ought to be exactly $-\varepsilon_{\mathrm{HOMO}}$ for an exact density functional. Note that all of the large-molecule excitation energies considered in this work fall below $-\varepsilon_{\mathrm{HOMO}}$. Consequently, these excitation energies are expected to be satisfactorily described by standard functionals.

One might hope that the LRC, which results in correct asymptotic behavior of v_{xc}, might provide $-\varepsilon_{\mathrm{HOMO}}$ values more in line with experimental ionization energies. Figure 16 shows $-\varepsilon_{\mathrm{HOMO}}$ as a function of μ for four of the molecules considered in Secs. III B and III C; the corresponding graphs for the other molecules are available in the Supporting Information.[34] The horizontal lines indicate the experimental ionization energies.[49] For each of the base ($\mu=0$) functionals, $-\varepsilon_{\mathrm{HOMO}}$ significantly underestimates the ionization energy, as expected. However, $-\varepsilon_{\mathrm{HOMO}}$ increases monotonically as a function of μ, and reaches the experimental ionization energy around $\mu \approx 0.4 a_0^{-1}$ for smaller molecules and $\mu \approx 0.25 a_0^{-1}$ for larger ones. As μ is increases further, the value of $-\varepsilon_{\mathrm{HOMO}}$ eventually plateaus, at a value substantially larger than the experimental ionization energy. We note that there appears to be some correlation (though it is not perfect) between the value of μ for which $-\varepsilon_{\mathrm{HOMO}}$ equals the ionization energy, and the value of μ that is optimal for TD-DFT vertical excitation energies.

V. CONCLUSIONS

Using the exchange kernel formulation of LRC-DFT proposed by Hirao and co-workers,[2–5] we have analyzed the performance of several LRC density functionals (both pure and hybrid), for calculation of ground-state properties (atomization energies, barrier heights, ionization energies, and electron affinities) as well as TD-DFT vertical excitation energies. Particular attention is paid to how each of these properties varies as a function of the range-separation parameter, μ. We find that statistical errors in most of the ground-state properties (save for ionization energies) are minimized using a value of μ that is significantly larger than the optimal value for excitation energies (see Tables I and II). Likewise, the value of μ that is optimal for excitation energies yields large statistical errors in ground-state atomization energies and barrier heights.

In addition, we find that the μ-dependence of small-molecule excitation energies (CO, H_2CO, and CH_3CO) is markedly different from that observed in larger molecules (anthracene, indole, pyridazine, benzocyclobutendione, benzaldehyde, and pyrrole). We attribute this difference to the fact that the valence excited-state densities for these larger molecules sample both the long- and short-range parts of the Coulomb potential, whereas the small molecules fit more or less within the length scale described using normal TD-DFT. These observations underscore the importance of having large-molecule excitation energies in the training set of any LRC functional that is intended for use in TD-DFT.

The range-separation parameter μ in LRC-DFT, much like the coefficient of HF exchange C_{HF} in hybrid DFT, offers the "opportunity" to tune the predicted values of most observables over a fairly wide range. In both cases, however, tuning a certain property in order to fit experimental data may seriously degrade a functional's ability to predict other important properties, and cannot be recommended as a computational strategy. The present study indicates that ground-state benchmarks of LRC-DFT are insufficient to insure that this method performs acceptably in TD-DFT calculations on larger molecules.

ACKNOWLEDGMENTS

This work was supported by a NSF CAREER award, by the ACS Petroleum Research Fund, and by start-up funds from The Ohio State University. Calculations were performed at the Ohio Supercomputer Center under Project No. PAS0291.

[1] P. M. W. Gill, R. D. Adamson, and J. A. Pople, Mol. Phys. **88**, 1005 (1996).
[2] H. Iikura, T. Tsuneda, T. Yanai, and K. Hirao, J. Chem. Phys. **115**, 3540 (2001).
[3] J.-W. Song, T. Hirosawa, T. Tsuneda, and K. Hirao, J. Chem. Phys. **126**, 154105 (2007).
[4] Y. Tawada, T. Tsuneda, S. Yanagisawa, T. Yauai, and K. Hirao, J. Chem. Phys. **120**, 8425 (2004).

[5] J.-W. Song, S. Tokura, T. Sato, M. A. Watson, and K. Hirao, J. Chem. Phys. **127**, 154109 (2007).

[6] J. Toulouse, F. Colonna, and A. Savin, Phys. Rev. A **70**, 062505 (2004).

[7] I. C. Gerber and J. G. Angyan, Chem. Phys. Lett. **415**, 100 (2005).

[8] I. C. Gerber, J. G. Angyan, M. Marsman, and G. Kresse, J. Chem. Phys. **127**, 054101 (2007).

[9] O. A. Vydrov and G. E. Scuseria, J. Chem. Phys. **125**, 234109 (2006).

[10] O. A. Vydrov, J. Heyd, A. V. Krukau, and G. E. Scuseria, J. Chem. Phys. **125**, 074106 (2006).

[11] T. M. Henderson, A. F. Izmaylov, G. E. Scuseria, and A. Savin, J. Chem. Phys. **127**, 221103 (2007).

[12] T. M. Henderson, B. G. Janesko, and G. E. Scuseria, J. Chem. Phys. **128**, 194105 (2008).

[13] T. Yanai, D. P. Tew, and N. C. Handy, Chem. Phys. Lett. **393**, 51 (2004).

[14] M. J. G. Peach, T. Helgaker, P. Salek, T. W. Keal, O. B. Lutnaes, D. J. Tozer, and N. C. Handy, Phys. Chem. Chem. Phys. **8**, 558 (2006).

[15] M. J. G. Peach, A. J. Cohen, and D. J. Tozer, Phys. Chem. Chem. Phys. **8**, 4543 (2006).

[16] A. W. Lange, M. A. Rohrdanz, and J. M. Herbert, J. Phys. Chem. B **112**, 6304 (2008).

[17] J.-D. Chai and M. Head-Gordon, J. Chem. Phys. **128**, 084106 (2008).

[18] A. Dreuw, J. L. Weisman, and M. Head-Gordon, J. Chem. Phys. **119**, 2943 (2003).

[19] R. J. Magyar and S. Tretiak, J. Chem. Theory Comput. **3**, 976 (2007).

[20] J. Plötner and A. Dreuw, Chem. Phys. **347**, 472 (2008).

[21] R. D. Adamson, J. P. Dombroski, and P. M. W. Gill, J. Comput. Chem. **20**, 921 (1999).

[22] A. Lange and J. M. Herbert, J. Chem. Theory Comput. **3**, 1680 (2007).

[23] D. Jacquemin, E. A. Perpète, G. Scalmani, M. J. Frisch, R. Kobayashi, and C. Adamo, J. Chem. Phys. **126**, 144105 (2007).

[24] D. Jacquemin, E. A. Perpète, O. A. Vydrov, G. E. Scuseria, and C. Adamo, J. Chem. Phys. **127**, 094102 (2007).

[25] D. Jacquemin, E. A. Perpète, G. E. Scuseria, I. Ciofini, and C. Adamo, J. Chem. Theory Comput. **4**, 123 (2008).

[26] Y. Shao *et al.*, Phys. Chem. Chem. Phys. **8**, 3172 (2006).

[27] A. D. Becke, Phys. Rev. A **38**, 3098 (1988).

[28] J. P. Perdew, K. Burke, and M. Ernzerhof, Phys. Rev. Lett. **77**, 3865 (1996).

[29] C. Adamo and V. Barone, J. Chem. Phys. **110**, 6158 (1999).

[30] C. Lee, W. Yang, and R. G. Parr, Phys. Rev. B **37**, 785 (1988).

[31] T. Tsuneda, T. Suzumura, and K. Hirao, J. Chem. Phys. **110**, 10664 (1999).

[32] B. J. Lynch and D. G. Truhlar, J. Phys. Chem. A **107**, 3898 (2003).

[33] Minnesota Database Collection, http://comp.chem.umn.edu/database (accessed May 18, 2008).

[34] See EPAPS Documents No. E-JCPSA6-129-601829 for additional basis set and excitation energy benchmarks. For more information on EPAPS, see http://www.aip.org/pubservs/epaps.html.

[35] P. M. W. Gill, B. G. A. Johnson, and J. Pople, Chem. Phys. Lett. **209**, 506 (1993).

[36] NIST Computational Chemistry Comparison and Benchmark Database, NIST Standard Reference Database No. 101, Release 14, September 2006 (http://cccbdb.nist.gov).

[37] Due to singlet-triplet instabilities in the LRC-BLYP calculations for ^{1}CH, this molecule is excluded from our results.

[38] Using LRC-BLYP, the transition state for reaction 6 in the database failed to converge for certain values of μ, so this reaction is omitted from our results.

[39] M. B. Robin, *Higher Excited States of Polyatomic Molecules* (Academic, New York, 1985), Vol. III.

[40] C. M. Hadad, J. B. Foresman, and K. B. Wiberg, J. Phys. Chem. **97**, 4293 (1993).

[41] E. S. Nielsen, P. Jørgensen, and J. Oddershede, J. Chem. Phys. **73**, 6238 (1980).

[42] A. Dreuw and M. Head-Gordon, Chem. Rev. (Washington, D.C.) **105**, 4009 (2005).

[43] M. Parac and S. Grimme, J. Phys. Chem. A **106**, 6844 (2002).

[44] M. van Faassen and P. L. de Boeij, J. Chem. Phys. **120**, 8353 (2004).

[45] Owing to convergence problems, the $\mu=0.33a_0^{-1}$ result for LRC-PBE and the $\mu=0.25a_0^{-1}$ result for LRC-PBE0 are not included in Fig. 9.

[46] A. Becke, J. Chem. Phys. **107**, 8554 (1997).

[47] C. Adamo, G. E. Scuseria, and V. Barone, J. Chem. Phys. **111**, 2889 (1999).

[48] M. E. Casida, C. Jamorski, K. C. Casida, and D. K. Salahub, J. Chem. Phys. **108**, 4439 (1998).

[49] NIST Chemistry WebBook, NIST Standard Reference Database Number 69, Released June 2005 (http://webbook.nist.gov/chemistry).